Measurement 252 (2025) 117356

Contents lists available at ScienceDirect

Measurement

journal homepage: www.elsevier.com/locate/measurement

High frequency eddy current method in inspection of aluminide coatings integrity after simulating service loads

Grzegorz Tytko [a], Małgorzata Adamczyk-Habrajska [b], Yong Li [c], Zenghua Liu [d], Mateusz Kopec [e,*]

[a] Faculty of Automatic Control, Electronics and Computer Science, Silesian University of Technology, 44-100 Gliwice, Poland
[b] Faculty of Science and Technology, University of Silesia, 41-500 Chorzów, Poland
[c] State Key Laboratory for Strength and Vibration of Mechanical Structures, Shaanxi Engineering Research Centre of NDT and Structural Integrity Evaluation, Xi'an Jiaotong University, Xi'an, Shaanxi, China
[d] School of Information Science and Technology. Beijing University of Technology, Beijing 100124, China
[e] Institute of Fundamental Technological Research Polish Academy of Sciences, Pawińskiego 5B, 02-106 Warsaw, Poland

ARTICLE INFO

Keywords:
Nickel alloys
Aluminide coating
Non-destructive testing
Eddy current testing

ABSTRACT

This study investigates the use of high-frequency eddy current testing (ECT) to assess the structural integrity of aluminide coatings on MAR-M247 nickel superalloy under simulated fatigue conditions. Aluminide coatings, deposited via chemical vapor deposition at thicknesses of 20 μm and 40 μm, were tested using custom-designed probes optimized for defect detection. Results demonstrate that substrate grain structure and coating thickness significantly influence coating durability, with fine-grain substrates exhibiting the least resistance changes and greatest fatigue tolerance. Eddy current signal variations correlated with microstructural changes, enabling detection of damage otherwise invisible to traditional methods. These findings establish ECT as a precise, non-destructive approach for monitoring aluminide coatings in critical applications.

1. Introduction

Nickel-based superalloys like MAR-M247 are indispensable in industries requiring materials capable of withstanding extreme temperatures and mechanical stresses, such as aerospace and power generation [1]. Their superior mechanical properties and resistance to thermal fatigue make them ideal for turbine blades and other high-stress components [2]. However, these materials are vulnerable to oxidation and corrosion in high-temperature environments, necessitating the application of protective coatings [3]. Aluminide coatings are widely utilized for this purpose, as they form a thermally stable alumina layer that provides excellent resistance to oxidative and corrosive degradation, thereby extending the operational lifespan of critical components [4]. The structural integrity of aluminide coatings directly impacts their protective efficacy [5]. Defects such as cracks, delamination, and thickness variations can compromise the coating's performance, leading to premature failure of the underlying substrate [6]. Ensuring the reliability of these coatings during production and throughout their service life is therefore essential [7]. Traditional methods of assessing coating integrity, such as metallographic analysis and scanning electron microscopy, offer valuable insights but are inherently destructive and time-consuming. These limitations render such methods unsuitable for routine inspections or for evaluating in-service components, particularly in high-value, large-scale systems.

Eddy current testing (ECT) has emerged as a powerful non-destructive evaluation method for characterizing defects and coatings, offering rapid, contactless, and precise measurements [8-11]. Based on the principle of electromagnetic induction, ECT involves inducing eddy currents in a conductive material using an alternating magnetic field. Variations in the material's properties, including electrical conductivity [12–14], magnetic permeability [15,16], and geometry [17–20], influence the distribution of these eddy currents and the impedance of the testing probe. Typically, the probe is in the form of a coil containing a ferrite core to increase its sensitivity and inspection efficiency [21–24]. For aluminide coatings, which are electrically conductive but non-magnetic, changes in coating thickness or the presence of defects alter the eddy current behavior, enabling the detection and characterization of such anomalies [7].

While previous studies have extensively examined the mechanical properties, oxidation resistance, and high-temperature performance of

* Corresponding author.
E-mail addresses: grzegorz.tytko@polsl.pl (G. Tytko), mkopec@ippt.pan.pl (M. Kopec).

https://doi.org/10.1016/j.measurement.2025.117356
Received 8 January 2025; Received in revised form 25 February 2025; Accepted 19 March 2025
Available online 22 March 2025

nickel-based superalloys, including MAR-M247, the application of non-destructive testing (NDT) techniques for assessing aluminide coatings remains an area of limited exploration. Traditional evaluation methods, such as metallographic analysis and scanning electron microscopy (SEM), have provided valuable insights into coating microstructure and failure modes but are inherently destructive, limiting their use for in-service inspections. Eddy current testing has been widely employed for flaw detection, conductivity measurements, and subsurface defect characterization in conductive materials. Several studies have demonstrated its effectiveness in detecting cracks, thickness variations, and material property changes in metallic structures. However, the application of ECT to aluminide coatings on MAR-M247 presents unique challenges, as these coatings are non-magnetic yet electrically conductive, requiring precise calibration of probe parameters to differentiate coating-specific defects from substrate effects. Existing research has primarily focused on ECT's ability to assess bulk material properties and multilayered conductive systems, but limited work has been conducted on optimizing ECT for thin protective coatings subjected to mechanical fatigue. Additionally, studies on ECT probe design and signal interpretation have largely been performed on standard geometries, with minimal attention given to the complex geometries of turbine components where edge effects and probe positioning significantly impact measurement accuracy.

This study advances the field by systematically investigating the influence of different grain structures—fine, coarse, and columnar—on the eddy current response of aluminide-coated MAR-M247 specimens. By analyzing how microstructural variations affect impedance changes under fatigue conditions, this research builds upon existing knowledge and refines ECT as a viable technique for non-destructive evaluation of coating integrity. Furthermore, the study addresses key gaps in probe optimization by developing and comparing two different probe designs (C14 and C18) to assess their effectiveness in mitigating edge effects and enhancing sensitivity. The identification of an optimal frequency range (11.84–12.06 MHz) for detecting coating degradation is another significant contribution, providing a more precise methodology for assessing structural changes in thin protective coatings. By bridging the knowledge gap between coating behavior under mechanical stress and the capabilities of ECT in detecting these changes, this research offers a novel and practical approach for ensuring the reliability and longevity of nickel-based superalloy components in aerospace and energy applications.

The application of ECT to aluminide coatings on MAR-M247 is a complex challenge due to the interaction of the coating's properties with those of the substrate. MAR-M247, a nickel-based superalloy with a high fraction of γ' precipitates, exhibits a complex microstructure that can affect electromagnetic signals. Moreover, surface conditions such as roughness or oxidation and the choice of testing parameters, including probe design and operating frequency, play a critical role in determining the method's sensitivity and accuracy. Proper calibration, accounting for these variables, is essential to ensure that the technique reliably differentiates between coating defects and substrate effects. By exploring the relationship between ECT signals and coating characteristics, it seeks to optimize the technique for detecting defects and ensuring uniformity. The research aims to enhance the understanding of coating-substrate interactions and demonstrate the potential of ECT as a tool for both manufacturing quality control and in-service maintenance. The insights gained will contribute to the broader adoption of non-destructive methods for safeguarding the performance and reliability of critical high-temperature components. It should be highlighted, that the presented methodology is not confined solely to the MAR M-247 nickel-based superalloy. The presented approach holds potential applicability across a broader spectrum of nickel-based superalloys with comparable chemical compositions. The paper's key innovation lies in the comprehensive investigation of three representative microstructures that are commonly observed in nickel-based superalloys, each of which is widely utilized in critical components of engines.

2. Materials and methods

2.1. Materials

Samples of the MAR-M247 nickel-based superalloy, prepared with three distinct microstructural variations – fine-grained, coarse-grained, and columnar – were fabricated using a conventional casting process (Fig. 1a-c). Aluminide coatings were subsequently deposited using the Chemical Vapor Deposition (CVD) method. The deposition was performed at 1040 °C in a hydrogen-enriched environment, maintaining an internal pressure of 150 mbar. Through precise optimization of the CVD process parameters, uniform coatings were achieved, with deposition times of 8 and 12 h producing layers of 20 μm and 40 μm thickness, respectively (Fig. 1d-e). When considering the industrial application of aluminide coatings, they are usually deposited to a thickness of up to 50 μm. Therefore, the authors selections of two intermediate values of these coating thicknesses fall within the range of their actual deposition.

2.2. Mechanical testing

The specimens for mechanical testing have the geometry presented in Fig. 2. The coated samples were subjected to cyclic fatigue loading using an MTS 810 machine, with tests performed at a frequency of 20 Hz, zero mean stress, and stress amplitudes between 300 MPa and 600 MPa. Such parameters were selected to represent the behavior of rotor components worked in engines. These tests were conducted at room temperature to replicate specific damage patterns typically observed in industrial turbine components. Fatigue testing was interrupted at 0.5 Nf to perform eddy current measurements.

2.3. EC measurements

The area selected for inspection is located at the narrowest part of the blade, which measures 15 mm in width and 52 mm in length (Fig. 2). In the middle of this section, a measurement point was established, which is the location where the probe was applied to the tested blade. Positioning the probe along the blade's symmetry axis (equidistant from both edges) allowed for the reduction of edge effects. Inspection area is significant due to its susceptibility to high stress concentrations, which are known to initiate cracking. The geometry of this section plays a crucial role in determining the optimal dimensions of the eddy current probe, ensuring effective coverage while minimizing measurement errors. To achieve optimal inspection results, the probe diameter must be carefully selected. The diameter should be large enough to enhance the inspection area and reduce the impact of external interference but still remain smaller than the width of the inspected section to mitigate edge effects that could skew the results. Based on these considerations, two absolute probes, labelled C14 and C18, were designed (Fig. 3). Each probe consisted of three key components: a coil, a core, and a head. The coils were wound with thin copper wire to achieve the maximum possible number of turns. Epoxy resin was applied to each layer of turns. This solution helped reduce the capacitance between the turns. Next, using the hot air soldering technique, the power supply wires were connected to the coil. The prepared coils were then affixed to the interior of the pot core and placed inside the head. The purpose of the head was to: protect the coil and core from mechanical damage, facilitate handling of the probe by the operator, and increase the precision of probe placement on the tested blade.

The smaller of the two probes (C14), with an outer core diameter of 14.2 mm, was designed to achieve the largest possible coil diameter. The critical limitation in this process was the edge effect on the sensitivity of the probe. Compensating this undesirable factor is especially important when testing narrow components, as this effect occurs simultaneously on both edges and significantly reduces the effectiveness of the inspection. Therefore, to determine the geometric dimensions of the coil, a numerical model was created using the Comsol Multiphysics package.

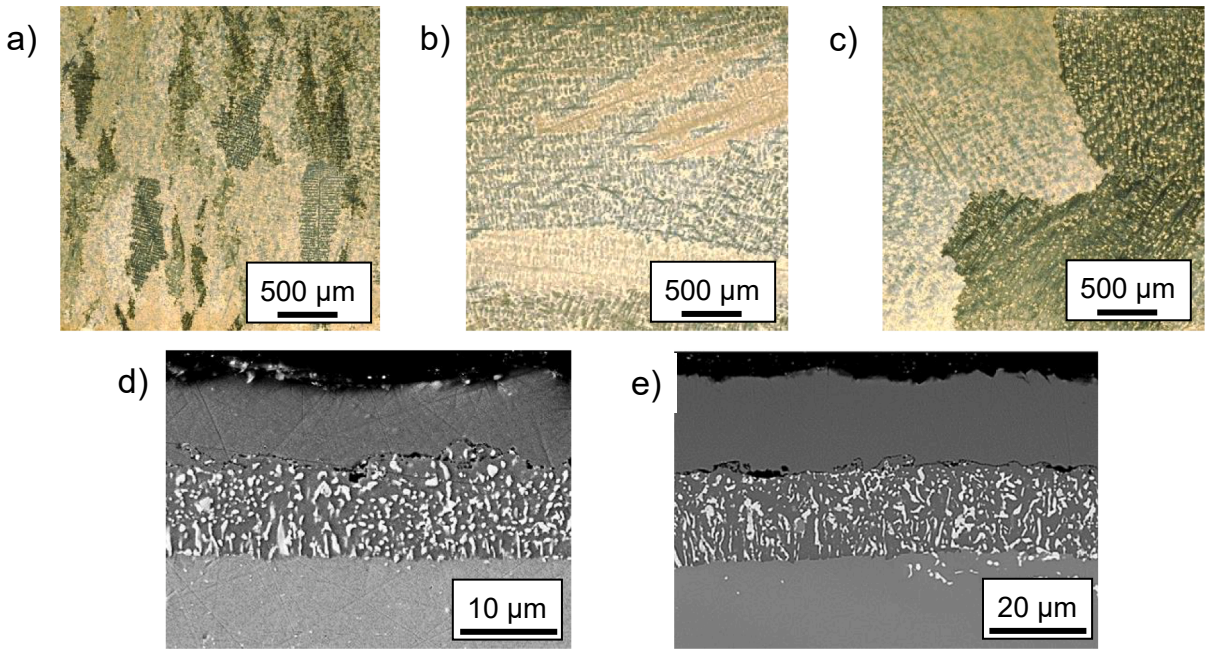

Fig. 1. Initial microstructures of MAR-M247 characterized by fine (a), column (b) and coarse (c) grains. Cross-sections of the MAR-M247 specimens with 20 μm (d) and 40 μm thick aluminide coatings (e).

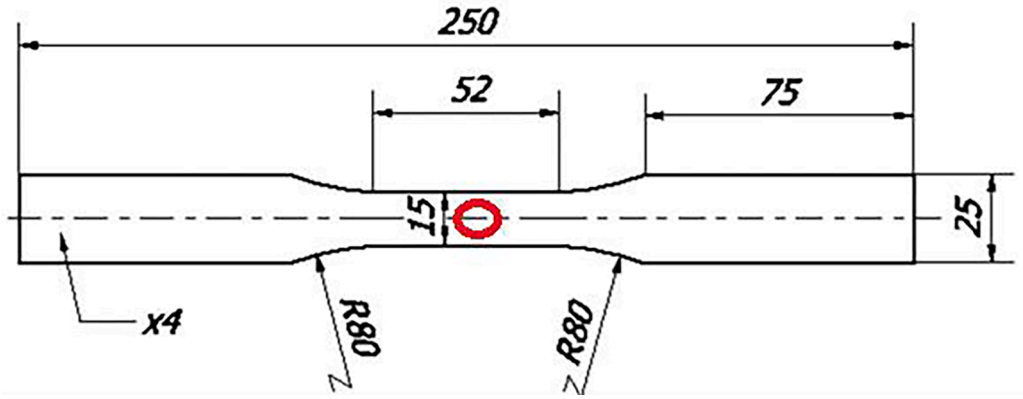

Fig. 2. Engineering drawing of the coated sample with the marked EC measurement area.

Fig. 3. Probe C18 (left), C14 (right) and gas turbine blade.

Using the finite element method, computer simulations were performed, allowing the optimal outer coil diameter of 11.6 mm to be determined. Increasing the coil diameter above this value leads to a decrease in probe sensitivity due to the increased impact of the edge effect on the probe's impedance. The critical value of the coil-to-blade edge distance, below which coatings of 20 μm and 40 μm thickness were indistinguishable, was found to be 0.5 mm. A slight margin was applied in the C14 probe, with a coil wound to an outer diameter of 11 mm. This coil, with a height of 2.7 mm and 740 turns, was then placed inside a pot core with an inner height of 3.0 mm and an outer height of 4.2 mm.

The larger of the two probes (C18) contains a pot core with an outer diameter of 18.2 mm, an inner height of 3.7 mm, and an outer height of 5.3 mm. Inside the core, a coil with an outer diameter of 14.8 mm and a height of 4.0 mm, containing 646 turns, was placed. C18 probe has a significantly larger coil area of 12.4 mm2 compared to the C14′s 6.35 mm2. This design aims to determine whether the increased coil area can counteract edge effect disturbances during impedance measurements, potentially offering enhanced performance compared to the smaller C14 probe. The two probes, C14 and C18, were developed to test different approaches for optimizing eddy current inspection. The C14 probe prioritizes precise placement and edge effect mitigation, while the C18 probe emphasizes increased sensitivity through its larger coil area. The interplay between probe geometry, coil size, and measurement accuracy was systematically analyzed to address the challenges posed by the geometry of the gas turbine blade. The gas turbine blade and the two probes are shown in Fig. 3, illustrating their respective designs and dimensions. These tools were selected and developed based on the specific requirements of the critical inspection area, aiming to provide reliable and accurate measurements while minimizing interference effects.

To improve the detection of structural changes in thin thermal barrier coatings, it is crucial to minimize magnetic flux dispersion into the surrounding environment. This was achieved using pot-core probes, which concentrate the magnetic flux within the probe core and direct it specifically toward the tested surface. By enhancing the magnetic flux penetrating the inspected material, the probe achieves higher impedance values, thereby improving signal clarity and minimizing the impact of external noise and interference during measurements. To examine structural changes in the coatings, the probe's operating frequency had to be carefully selected to match the eddy current penetration depth to the coating thickness. A frequency was chosen that allowed the eddy currents to penetrate slightly beyond the coating layer, including the critical interface between the coating and substrate, without extending into deeper substrate regions. This ensured that the substrate's electromagnetic influence did not overshadow the coating's response.

Impedance measurements were conducted using a high-precision Agilent 4294A impedance analyzer, with an accuracy of ±0.08 %. The analyzer was connected to an Agilent measurement fixture and 16,048 cables designed for use with the 4294A device, characterized by low signal transmission losses. The analyzer calibration was then performed in three stages. In the first step, calibration was conducted for open measurement terminals (open mode). In the next step, the measurement terminals were shorted (short mode). The final stage involved calibration with the connection of a stable reference resistor made from a specially selected alloy, with a resistance value close to that of the probe. The applied resistor featured silver-plated tellurium copper binding posts and exhibited no measurable influence from temperature hysteresis and ambient pressure. The resistor was connected using copper, screened Teflon cables.

After calibration, the probe was connected to the analyzer. An increase in cable length could lead to an increase in measurement error. For this reason, compensation for the influence of the probe cables on measurement accuracy was performed. Automatic mechanisms available in the analyzer were used for this purpose. These procedures trigger the measurement of the probe's impedance components and subsequently perform calculations, taking into account the known error for the 16,048 cable without the probe connected. To enhance reliability, the probe impedance was calculated as the average of eight measurements taken at 1-second intervals. Initial tests were performed across a broad frequency range of 1 MHz to 25 MHz, by using swept frequency technique [25–28]. The probe was stimulated with a sinusoidal signal. The results showed that the probe was most sensitive to changes in impedance within a narrow frequency range of approximately 11.8 MHz to 12.1 MHz. For this frequency range, the standard penetration depth was 30 μm. This value is intermediate between the thicknesses of the tested coatings, which were 20 μm and 40 μm. The total penetration depth of eddy currents is slightly greater, as this parameter defines the depth at which the eddy current density is 37 % of the value achieved at the material surface. Next, final measurements were conducted at 100 specific frequencies between 11.5 MHz and 12.5 MHz, enabling detailed and accurate assessments of the coating's structural condition. This methodology highlights the importance of selecting optimal probe configurations and operating parameters to ensure accurate detection of structural variations in thin coatings, especially when examining critical layers like the coating-substrate interface.

After determining the operational frequency range of the probe, impedance measurements were carried out at as-received, non-defected blades with TBC coatings of 20 μm and 40 μm thickness. The purpose of these tests was to verify the accuracy of the performed computer simulations and to compare the sensitivity of both probes, taking into account the edge effect. Probes C14 and C18 were positioned on the symmetry axis of the blade, at a location with a width of 25 mm. The obtained reactance changes were small, while the resistance changes were significant. The sensitivity of probe C18 was higher than that of probe C14. Subsequently, measurements were performed at the narrowest section of the blade, with a width of 15 mm (the measurement point is indicated by a red circle in Fig. 2). The reactance changes for both coils were very small. The resistance changes for probe C14 were large, in contrast to the small resistance changes of probe C18, which made it difficult to clearly differentiate coatings of different thicknesses. Therefore, the measurement results led to the following conclusions:

- In all cases, very small changes in the reactance of both probes were observed, which suggests that this parameter will not be considered in further tests.
- Probe C18 exhibited greater sensitivity than probe C14 for impedance component measurements at the 25 mm wide section of the blade.
- The outer diameter of the coil in probe C18 was too large for measurements at the 15 mm wide section of the blade. In these tests, the strong interaction of both blade edges caused the resistance changes of the probe to be small, making it impossible to distinguish between the tested coatings.

As a result, probe C18 was excluded from further tests in favor of probe C14, which demonstrated significant resistance changes in all measurement configurations. The use of high operational frequency for the probe requires compensation for the influence of unwanted factors on measurement results. One of the most commonly applied solutions is based on changes in the measured parameter value of the probe. In the case of impedance, the measurement is first performed without the presence of a conductive material (Z_0), followed by measurements with the probe positioned at its target location, in contact with the tested element (Z). Determining the change in impedance as the difference between these two values ($Z - Z_0$) should reduce errors caused by unwanted factors. Based on the performed measurements, it was concluded that, at such a high frequency range, this approach is insufficient because unwanted factors affect impedance Z_0 differently than impedance Z. The authors believe that the most significant impact on measurement errors stems from capacitive effects, including parasitic capacitance. It was observed that this effect is much larger for complex signals (such as impedance or phase shift) than for real signals. Moreover, capacitive effects most strongly affect the imaginary part of the

signal. In the case of impedance measurements, this causes the changes in reactance to be significantly smaller than the changes in resistance during tests. For these reasons, in subsequent research, the authors focused on an analysis based solely on the real signal, choosing to measure the resistance value of the probe. Both the designed probes and the tested blades have flat surfaces, ensuring their mutual contact during tests. This prevents the probe from tilting, and the probe's lift-off distance from the tested surface does not exceed 0.1 mm. In practical applications, it is recommended to use attachments or holders that enable precise positioning of the probe at the measurement point and stabilization of its position. These elements can have universal geometric dimensions due to the same width of the blade at the inspection location, which is 15 mm. The use of a holder or attachment not only reduces the impact of the lift-off and probe tilt effects but also mitigates the edge effect by positioning the probe at an equal distance from both blade edges. To determine the changes in resistance obtained during the measurements of two samples, the relative change in resistance, δR, expressed as a percentage, was defined. The maximum value of this parameter was denoted as δR_{MAX}.

$$SR = \left|\frac{R_1 - R_2}{R_1}\right| \cdot 100\% \quad (1)$$

2.4. Microstructural observations

Microstructural observations were performed in the area of effective gauge length located in the central section of the specimen presented in Fig. 2. Both, optical (Nikon MA220) and scanning electron microscopes (JEOL 6360) were used to analyze the cross-section and fracture surfaces of specimens.

3. Results and discussion

3.1. EC measurements

Gas turbine blades made of MAR-M247 nickel superalloy, coated with thermal barrier coatings (TBC), were subjected to fatigue tests with stress amplitudes ranging from 350 to 600 MPa. Following the fatigue testing, measurements of the resistance of an eddy current probe (C14 model) were conducted by placing the probe in contact with the narrowest section of the blade, which had a width of 15 mm. The results obtained are presented in Fig. 4 and Table 1.

The fatigue tests were performed to evaluate the durability of the TBC coatings. The most durable coatings exhibited significantly less damage during the fatigue tests compared to coatings with lower durability. Any mechanical damage to the coating that induces structural changes also affects the resistance of the probe. Cracks, delamination, fissures, and other material defects occurring within the coating structure or at its interface with the MAR-M247 substrate disturb the flow of eddy currents. This disruption in the eddy current distribution alters the magnetic field intensity, resulting in changes in the probe resistance. Consequently, the expected relative probe resistance difference δR should be minimized for optimal performance.

The presented data indicate that the largest resistance changes were observed for coatings on substrates with a columnar grain structure, while the smallest changes were found for substrates with a fine grain structure. Moreover, the fine grain structure demonstrated the least sensitivity to changes in the fatigue test amplitude on the maximum

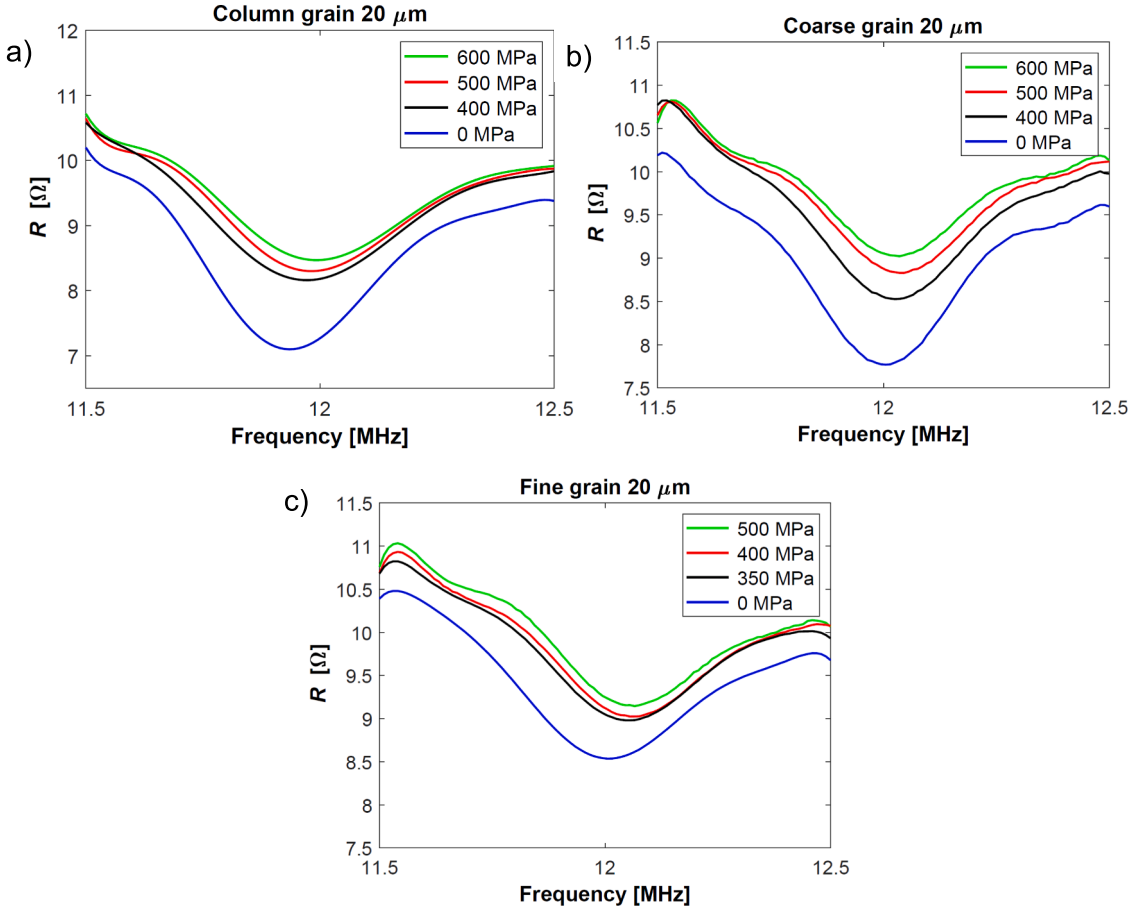

Fig. 4. Resistance evolution registered for column (a), coarse (b) and fine (c) grained samples with 20 μm coating subjected to fatigue tests at different stress amplitudes in comparison to non-deformed state.

Table 1
Resistance and δR_{MAX} coefficient values for specimens with different initial microstructure and 10 μm thick aluminide coating (R_1 – resistance of the first sample, R_2 – resistance of the second sample).

MAR-M247 microstructure	First sample	Second sample	Frequency [MHz]	R_1 [Ω]	R_2 [Ω]	δR_{MAX} [%]
Column grain	0 MPa	400 MPa	11.84	7.46	8.58	15.0
	0 MPa	500 MPa	11.87	7.27	8.62	18.6
	0 MPa	600 MPa	11.85	7.35	8.91	21.2
Coarse grain	0 MPa	400 MPa	11.98	7.79	8.68	11.4
	0 MPa	500 MPa	11.98	7.79	8.90	14.2
	0 MPa	600 MPa	11.96	7.82	9.14	16.9
Fine grain	0 MPa	350 MPa	11.89	8.74	9.52	8.9
	0 MPa	400 MPa	11.89	8.74	9.62	10.1
	0 MPa	500 MPa	11.89	8.74	9.76	11.7

value of the relative resistance difference, defined as δR_{MAX}. When the amplitude increased from 400 MPa to 500 MPa, the δR_{MAX} values changed by 3.6 % (column grain), 2.8 % (coarse grain), and only 1.6 % for fine grain. These results, obtained for coatings with a thickness of 20 μm, indicate that the coatings deposited on fine grain substrates exhibited the highest durability under fatigue testing conditions, whereas the coatings on column grain substrates showed the lowest durability.

In all the tested samples, even relatively low stress amplitudes in the range of 350–400 MPa caused significant changes in probe resistance R, ranging from approximately 9 % to 15 %. Such high δR_{MAX} values enable a clear distinction between samples subjected to fatigue processes and reference samples (0 MPa). The adopted stress amplitude range (350–600 MPa) induced structural changes both in the TBC coating and in the substrate, negatively affecting the gas turbine blade properties and potentially leading to blade failure. Notably, these structural changes were not visible on the surface of the blade and could not be detected using conventional visual inspection methods.

In the next step, measurements were conducted for blades coated with a 40 μm thick layer. The results obtained for the columnar grain structure are presented in Fig. 5 and Table 2. A significant difference in probe resistance was observed between the reference sample (0 MPa)

Table 2
Probe resistance and δR_{MAX} coefficient values for column grained samples with 40 μm thick coating (R_1 – resistance of the first sample, R_2 – resistance of the second sample).

First sample	Second sample	Frequency [MHz]	R_1 [Ω]	R_2 [Ω]	δR_{MAX} [%]
0 MPa	300 MPa	11.91	8.33	10.33	24.0
0 MPa	450 MPa	11.91	8.33	10.52	26.3
0 MPa	500 MPa	11.91	8.33	10.61	27.4

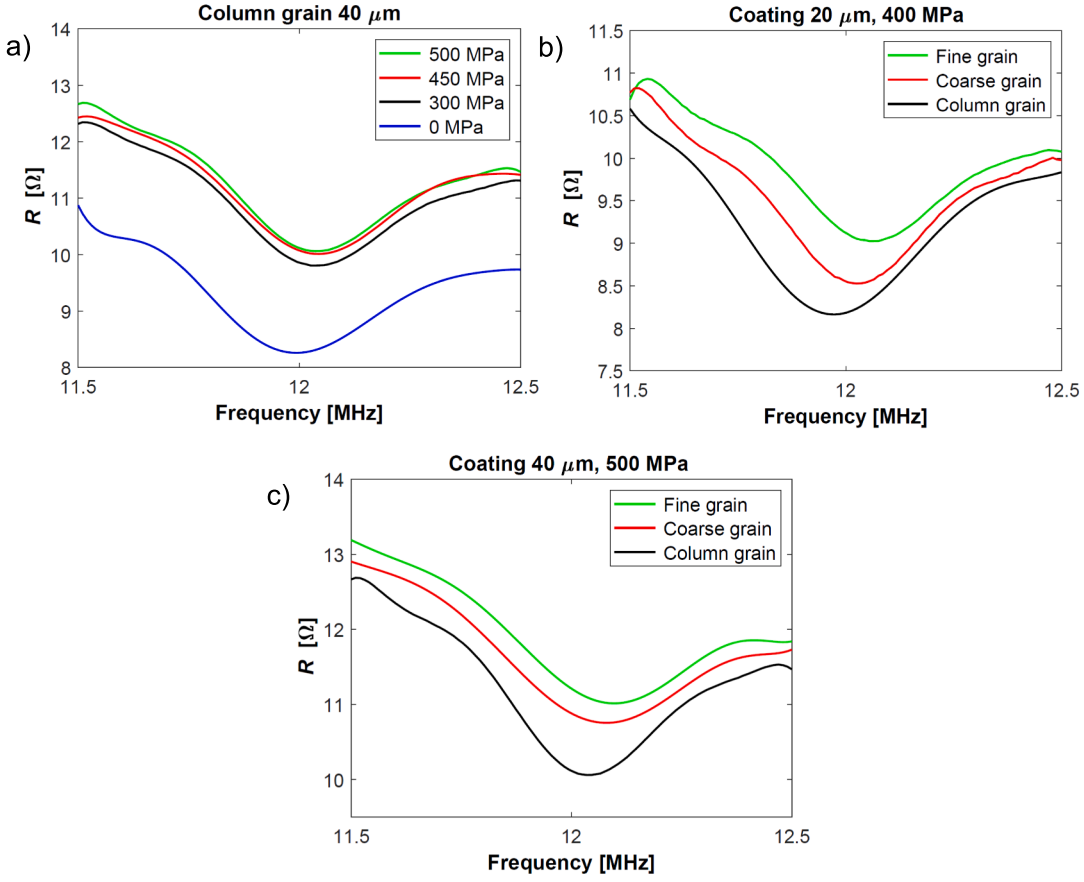

Fig. 5. Resistance evolution for column grained samples with a 40 μm coating, subjected to fatigue tests at different stress amplitudes (a); Resistance evolution for samples with a 20 μm coating, subjected to fatigue tests at stress amplitude equal to 400 MPa (b); Resistance evolution for samples with a 40 μm coating, subjected to fatigue tests at stress amplitude equal to 500 MPa (c).

and the samples subjected to fatigue testing across the entire frequency range of 11.5 MHz to 12.5 MHz. Furthermore, increasing the stress amplitude only slightly affected the δR coefficient. Specifically, changing the stress amplitude from 300 MPa to 500 MPa resulted in a δR_{MAX} change of just 3.4 %. At the same time, the δR_{MAX} values achieved were notably high, ranging from 24 % to 27.4 %. These results indicate substantial degradation of the 40 μm thick coating. The extent of damage is so significant that further increases in stress amplitude no longer cause meaningful structural changes in the coating. Therefore, it can be concluded that the coating has lost its functional properties and is no longer fulfilling its intended purpose.

In Fig. 6, the changes in probe resistance are compared for samples with different substrate structures subjected to fatigue testing at stress amplitudes of 400 MPa and 500 MPa, respectively. The probe resistance values for 40 μm thick coatings were higher than those for 20 μm thick coatings. This trend was also observed for samples that were not subjected to fatigue testing (Figs. 4-5). It was further determined that, across all tested samples, the highest resistance values R were recorded for fine-grain substrates, while the lowest were observed for column-grain substrates. However, the absolute resistance values of the probe do not allow for a direct assessment of coating durability. A more reliable parameter for this evaluation is the difference in resistance values. To assess coating durability, the values of the δR coefficient were analyzed for samples with 20 μm and 40 μm coatings subjected to fatigue testing at a 500 MPa amplitude (Fig. 6). The highest values of this coefficient for various samples are presented in Table 3. For 20 μm thick coatings, the δR_{MAX} values were the smallest, indicating that these coatings exhibited greater resistance to fatigue testing compared to the 40 μm thick coatings. Regardless of the coating thickness, the best results were obtained for fine-grain substrates, while the worst were observed for column-grain substrates. The differences in results between samples with different substrate structures were significant for 20 μm coatings but much smaller for 40 μm coatings. Additionally, it was noted that for 20 μm thick coatings, the δR_{MAX} value typically reached a distinct maximum, around which its value significantly decreased. In contrast, much smaller changes in this parameter were observed for 40 μm coatings, where the influence of the probe's operational frequency was less pronounced. A detailed analysis conducted using microscopy revealed the cause of these differences. The structure of the 20 μm coatings experienced less damage than the 40 μm coatings. However, the

Table 3
Probe resistance values and δR_{MAX} coefficient for samples with 20 μm and 40 μm coatings subjected to fatigue tests at stress amplitude of 500 MPa.

Coating thickness	20 μm	20 μm	20 μm	40 μm	40 μm	40 μm
Grain structure	Column	Coarse	Fine	Column	Coarse	Fine
δR_{MAX} [%]	18.6	14.2	11.7	27.4	24.9	23.9

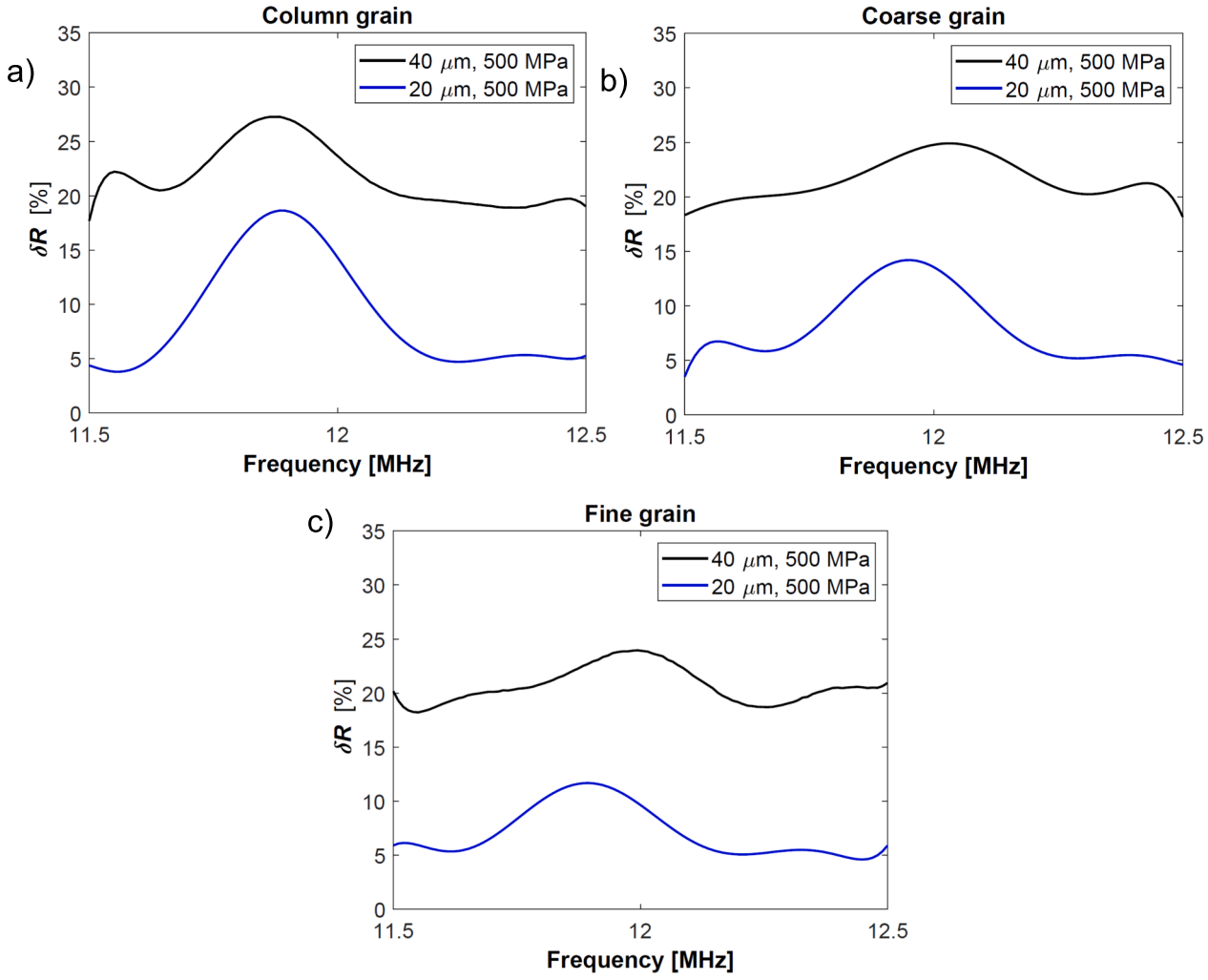

Fig. 6. Resistance coefficient δR changes registered for column (a), coarse (b) and fine (c) grained samples with 20 μm and 40 μm coatings subjected to fatigue tests at stress amplitude equal to 500 MPa.

thinner coating resulted in more pronounced changes at the coating-substrate interface, where the largest differences between samples with different substrate structures were also observed. The coating-substrate interface significantly influenced the change in probe resistance for 20 μm coatings. This effect was most pronounced only within a narrow range of optimal probe operating frequencies, where the penetration depth of eddy currents was neither too large nor too small. Conversely, the damage in thicker coatings caused by fatigue testing was substantial enough to have a greater impact on resistance changes than the coating-substrate interface. As a result, the decrease in δR_{MAX} was smaller than for thinner coatings, and the δR parameter maintained high values over a broader frequency range. These findings suggest that the behavior of probe resistance is strongly influenced by the interaction of coating thickness, substrate structure, and probe operating frequency. The thinner coatings, while less damaged overall, exhibit greater sensitivity to changes at the interface, particularly under finely tuned frequency conditions. In contrast, thicker coatings experience more uniform damage, which dominates resistance changes, leading to a broader frequency response range.

The conducted studies on gas turbine blade coatings, which were previously subjected to fatigue testing, were performed using a custom-designed C14 probe. The measurements of the probe's resistance led to several key conclusions: all fatigue-tested samples could be effectively differentiated from reference samples based on aluminide coating measurements; an increase in stress amplitude during fatigue testing resulted in a higher resistance difference compared to the reference

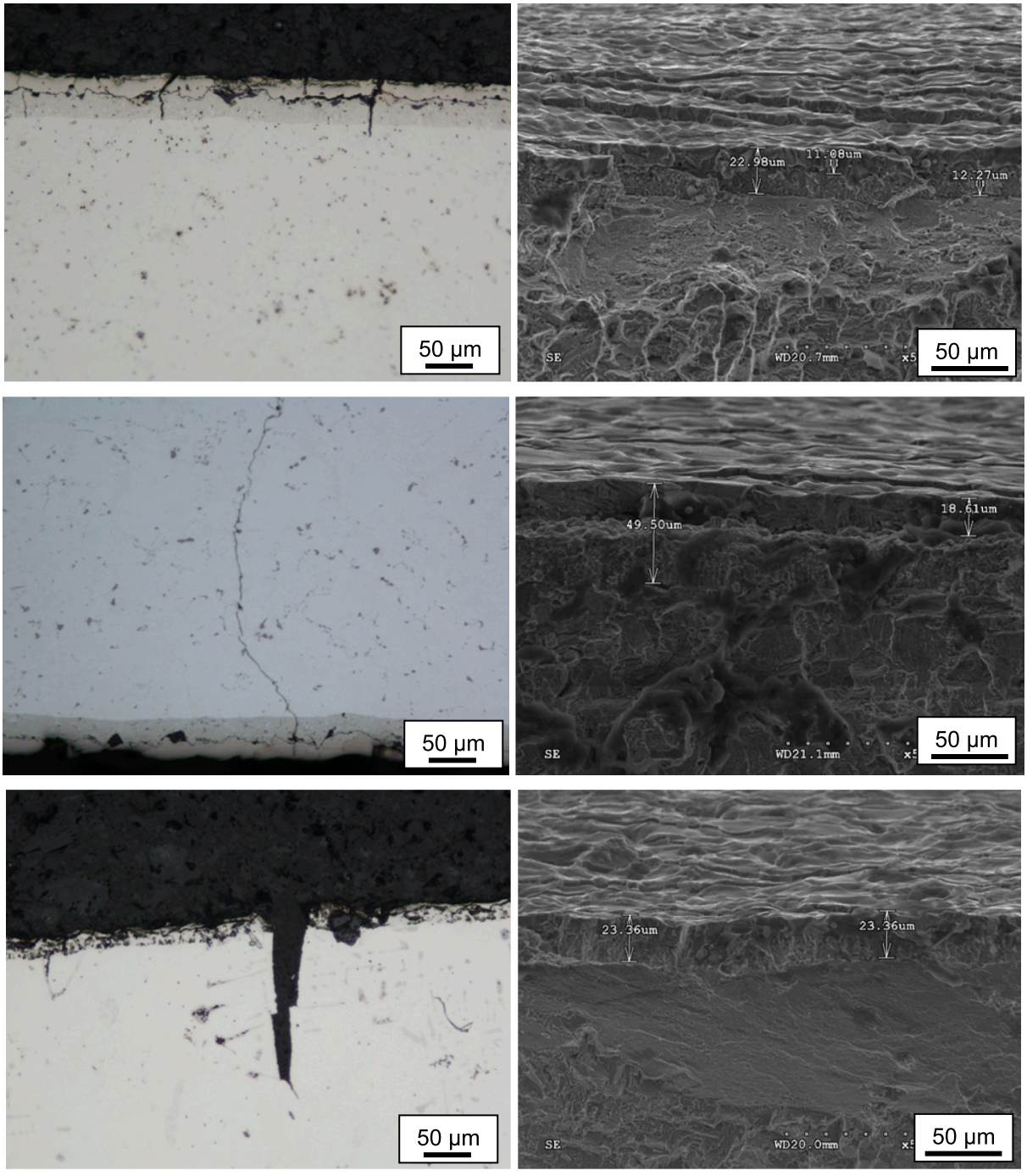

Fig. 7. Cross-sectional and side view of MAR-M247 with fine (a), coarse (b) and column (c) subjected to fatigue at a stress amplitude of 400 MPa.

samples; coatings with a thickness of 20 μm showed smaller structural changes compared to thicker coatings; the smallest resistance changes, indicating the highest durability, were found in samples with a fine-grain substrate structure, while the largest resistance changes were observed in samples with a columnar-grain substrate; the greatest resistance differences were recorded in a narrow frequency range of 11.84 MHz to 12.06 MHz, which helped identify optimal testing parameters; and it was demonstrated that eddy current inspection can detect structural changes in thin aluminide coatings applied to MAR-M247 nickel alloy substrates.

3.2. Microstructural aspects in EC measurements

Fatigue crack initiation in MAR-M247 under cyclic loading is a complex process that depends on microstructural characteristics, stress distribution, and coating-substrate interactions [3]. The substrate's grain structure plays a critical role in determining coating durability, influencing how stresses are transmitted and localized at the interface. In equiaxed grain structures, the presence of numerous grain boundaries acts as stress concentration sites, leading to localized plastic deformation and early crack initiation [29]. These grain boundaries could also create mismatch stresses between the coating and the substrate, promoting interfacial decohesion and accelerating failure mechanisms such as delamination and spallation. Such behavior could be related to the coarse and fine microstructure of MAR-M247 (Fig. 1a,c), where the developed microstructure could be observed below fractured coating. Although some of these features could be observed on fracture surfaces (Fig. 7a,b), one should highlight, that the aluminide coatings exhibit great adhesion to the substrate material as even after fracture, they adhere to MAR-M247 well. Additionally, the crack initiation may be observed on the side of specimens, where the coating is present. It can be clearly observed in Fig. 7a, that even though multiple cracks appear in the coating, only one dominant crack appeared in the substrate material. It could be concluded that the coating itself transfers some loading during service therefore, the necessity of inspection of these coatings through ETC was confirmed. On the other hand, solidified, column structure (Fig. 7c) provides enhanced coating performance by reducing the number of transverse grain boundaries, thereby minimizing stress localization and improving coating adhesion. It exhibits the best fatigue resistance due to the absence of grain boundaries, which significantly reduces stress concentrations and enhances load transfer between the substrate and the coating.

Internally, coatings on MAR-M247 experience various microstructural changes during cyclic loading, which affect their durability. Crack formation is a primary concern, typically originating at pre-existing pores, oxide inclusions, or weak interfacial regions [1–3]. These cracks tend to propagate along the coating-substrate interface or through the coating itself, depending on the level of adhesion and the inherent strength of the material. Porosity within the coating acts as a preferential site for crack initiation and growth. Increased cyclic loading exacerbates this issue by causing microcrack coalescence, which eventually leads to spallation or coating detachment. Furthermore, interfacial bonding strength plays a crucial role in determining coating longevity—strong metallurgical bonding reduces susceptibility to early delamination, while weaker adhesion, influenced by factors such as oxidation and thermal mismatch stresses, leads to premature coating failure. These microstructural degradations, including crack propagation, porosity evolution, and coating delamination, can be effectively characterized using eddy current testing [30]. This NDE technique detects variations in electrical conductivity and impedance caused by internal defects. As cracks grow and porosity increases, localized disruptions in conductivity become more pronounced, altering the eddy current response. Changes in signal amplitude and phase shift can be correlated with damage severity, allowing for real-time monitoring of coating integrity. Additionally, differences in grain structure influence eddy current measurements, as column structures exhibit more uniform conductivity, while equiaxed structures show greater variability due to the presence of grain boundaries. By integrating eddy current analysis with microstructural examinations, it is possible to develop predictive models for fatigue failure in MAR-M247 coatings, improving maintenance strategies and extending component lifespan in high-temperature applications.

3.3. Discussion on applicability and limitations

The study's focus on MAR-M247 nickel-based superalloy and aluminide coatings provides valuable insights into the effectiveness of ECT for detecting coating degradation. However, the findings cannot be directly generalized to all nickel-based alloys and coating systems without further investigation. Nickel-based superalloys such as Inconel 718, Rene 80, and CMSX-4 possess different microstructural characteristics, and conductivity which influence their behavior under cyclic loading and their interaction with ECT signals [31]. For example, Inconel 718 contains a significant amount of γ'' phase, which provides excellent strength but differs in fatigue resistance from the γ' phase-dominated MAR-M247. The variation in electrical conductivity and magnetic permeability of these alloys may affect the impedance response in ECT, requiring recalibration of probe settings and signal interpretation methods to ensure accurate defect detection [32]. Similarly, other protective coatings, such as MCrAlY (where M = Ni, Co, or Fe) or thermal barrier coatings (TBCs) made of Yttria-Stabilized Zirconia (YSZ), exhibit different electrical, mechanical, and oxidation behaviors. Aluminide coatings primarily provide oxidation resistance through the formation of an alumina layer, whereas MCrAlY coatings offer additional protection against both oxidation and hot corrosion, making them suitable for marine and industrial gas turbine applications. In contrast, TBCs function as thermal insulators and often experience failure mechanisms such as spallation due to thermal expansion mismatches. Since ECT is sensitive to electrical conductivity changes, its effectiveness in detecting defects in these coatings would depend on their unique properties.

The simulated fatigue conditions used in this study—uniaxial cyclic loading at room temperature—provide a controlled environment to analyze coating degradation but do not fully replicate the complex service conditions encountered in real-world applications. Components in aerospace, power generation, and industrial gas turbines operate under highly variable and challenging conditions, including multi-axial loading, thermo-mechanical fatigue (TMF), and environmental degradation [33]. In practical applications, mechanical components experience a combination of tensile, compressive, shear, and torsional stresses rather than simple uniaxial loading [34]. Turbine blades, for example, undergo centrifugal forces, aerodynamic loading, and vibrational stresses, leading to multi-axial stress states that affect fatigue crack initiation and propagation differently from the conditions simulated in the study. Future studies should incorporate multi-axial fatigue testing by applying combined bending, torsion, and tension loads to more accurately replicate real-world service conditions. This would help determine whether ECT remains effective for detecting coating degradation under these more complex stress states. Additionally, nickel-based superalloys and their coatings are typically exposed to high temperatures (800–1100 °C) and cyclic thermal stresses, which induce oxidation, creep, and phase transformations [1,2]. The combination of mechanical fatigue and thermal cycling—known as thermo-mechanical fatigue (TMF)—plays a crucial role in the degradation of coatings. To address such issues, the future research should include high-temperature TMF testing, where specimens are subjected to both mechanical cycling and controlled thermal cycles to simulate actual turbine operating conditions. This would provide more accurate insights into how coatings degrade over long-term service and whether ECT can reliably detect damage in such environments. One should mentioned, that real-world applications expose coated components to oxidizing environments, combustion gases, and corrosive contaminants (e.g., sulfur, vanadium,

and alkali metal salts), which contribute to coating degradation. The interaction between fatigue and oxidation can lead to accelerated crack growth, making it essential to assess how these effects influence ECT measurements. Future work could integrate oxidation testing and in-situ ECT monitoring to observe how oxidation-induced changes affect impedance readings. This would ensure that ECT remains effective under real-world environmental conditions. Finally, turbine components, such as blades and vanes, often feature curved, complex geometries that can introduce measurement inaccuracies due to edge effects and variations in probe positioning. The study primarily investigates flat, controlled surfaces, but real-world inspections require ECT probes that can adapt to non-uniform surfaces while maintaining sensitivity. To further expand the possibilities of presented methodology, flexible or conformal ECT probes will be designed. Those should possibly integrate array-based sensors that can scan irregular surfaces while compensating for variations in probe orientation.

4. Conclusions

In this paper, the integrity of aluminide coatings after simulating operational loading conditions was investigated using the eddy current method. The proposed technique required the simultaneous fulfillment of several critical requirements to ensure effective, rapid, and cost-efficient inspections within the high-frequency range. Firstly, the high sensitivity of the probe required for testing thin coatings was achieved by introducing proprietary solutions into the design process and using a pot core. Secondly, the edge effect was minimized by selecting optimal geometric dimensions for the probe and precisely determining the measurement points. Then, a narrow range of operational frequencies corresponding to the coating thickness was identified, in which the probe sensitivity was maximized. Subsequently, the influence of unwanted capacitive effects was reduced by analyzing only the real part of the impedance measurement results. Finaly, measurement accuracy was improved by conducting a three-step calibration of the measuring device and compensating for the influence of the probe's power supply cables. The completion of all the above procedures enabled the effective application of the developed technique for eddy current testing of coating structures.

Based on the obtained results, the following conclusions were formulated:

- High-frequency ECT (11.84–12.06 MHz) successfully detected coating degradation, with δR_{MAX} variations from 11.7 % to 27.4 %, confirming its suitability for non-destructive evaluation.
- 20 μm coatings showed better fatigue resistance than 40 μm coatings, with δR_{MAX} increasing by 3.4 % at higher stress (300–500 MPa), indicating greater structural stability.
- Fine-grained substrates exhibited the least resistance change (~1.6 %), while columnar grains showed the highest degradation (up to 27.4 % δR_{MAX} at 500 MPa), confirming fine grains enhance durability.
- Even at 350–400 MPa, ECT detected 9–15 % resistance changes, proving its sensitivity to early-stage damage, including microcracks and delamination.
- ECT is a fast, reliable tool for monitoring coating integrity in aerospace and energy applications. Fine-grain substrates with thinner coatings provide optimal fatigue resistance, extending component lifespan.

CRediT authorship contribution statement

Grzegorz Tytko: Writing – review & editing, Writing – original draft, Visualization, Validation, Supervision, Methodology, Investigation, Funding acquisition, Formal analysis, Data curation, Conceptualization. **Małgorzata Adamczyk-Habrajska:** Methodology, Investigation. **Yong Li:** Supervision, Validation. **Zenghua Liu:** Validation, Supervision, Software. **Mateusz Kopec:** Writing – review & editing, Writing – original draft, Visualization, Validation, Supervision, Resources, Project administration, Investigation, Funding acquisition, Formal analysis, Data curation, Conceptualization.

Declaration of competing interest

The authors declare that they have no known competing financial interests or personal relationships that could have appeared to influence the work reported in this paper.

Acknowledgements

The authors would like to express their gratitude to Mr M. Wyszkowski and Prof. D. Kukla for their kind help during the experimental part of this work.

Data availability

Data will be made available on request.

References

[1] I. Šulák, K. Obrtlík, Thermomechanical and isothermal fatigue properties of MAR-M247 superalloy, Theor. Appl. Fract. Mech. 131 (2024) 104443, https://doi.org/10.1016/j.tafmec.2024.104443.
[2] I. Šulák, K. Obrtlík, AFM, SEM AND TEM study of damage mechanisms in cyclically strained mar-M247 at room temperature and high temperatures, Theor. Appl. Fract. Mech. 108 (2020) 102606, https://doi.org/10.1016/j.tafmec.2020.102606.
[3] I. Šulák, K. Obrtlík, L. Čelko, P. Gejdoš, D. Jech, High-temperature low-cycle fatigue behaviour of mar-m247 coated with newly developed thermal and environmental barrier coating, Adv. Mater. Sci. Eng. (2018), https://doi.org/10.1155/2018/9014975.
[4] M. Kopec, Recent advances in the deposition of aluminide coatings on nickel-based superalloys: a synthetic review (2019–2023), Coatings 14 (5) (2024) 630, https://doi.org/10.3390/coatings14050630.
[5] M. Kopec, Effect of aluminide coating thickness on high-temperature fatigue response of MAR-M247 nickel-based superalloy, Coatings 14 (2024) 1072, https://doi.org/10.3390/coatings14081072.
[6] V.S. Shalaka, S. Sanjay, Interplay between cracking and delamination in incrementally deposited plasma sprayed coatings, Acta Mater. 215 (2021) 117074, https://doi.org/10.1016/j.actamat.2021.117074.
[7] G. Tytko, M. Adamczyk-Habrajska, Y. Luo, M. Kopec, Eddy current testing in the quantitive assessment of degradation state in MAR247 nickel superalloy with aluminide coatings, J. Nondestruct. Eval. 43 (2024) 112, https://doi.org/10.1007/s10921-024-01129-x.
[8] G. Tytko, Eddy current testing of small radius conductive cylinders with the employment of an I-core sensor, Measurement 186 (2021) 110219, https://doi.org/10.1016/j.measurement.2021.110219.
[9] G. Tytko, Measurement of multilayered conductive discs using eddy current method, Measurement 204 (2022) 112053, https://doi.org/10.1016/j.measurement.2022.112053.
[10] S. Zhang, Analytical model of an E-core driver-pickup coils probe applied to eddy current testing of multilayer conductor, ACES Journal 38, 11 (2023) 914, https://doi.org/10.13052/2023.ACES.J.381110.
[11] S. Saibo, Z. Xinnan, Z. Xun, Y. Kuohai, et al., Simultaneous carbon fiber layer thickness and direction measurement and identification using a novel eddy current sensor and simplified multi-scale 1D-ResNet network, Measurement 242 (Part A) (2025), https://doi.org/10.1016/j.measurement.2024.115812.
[12] H. Ma, D. Wang, Z. Zhang, W. Yin, H. Chen, G. Zhou, A simple conductivity measurement method using a peak-frequency feature of ferrite-cored eddy current sensor, NDT and E Int. 142 (2024) 103024.
[13] Y. Liu, Z. Zhang, W. Yin, A novel conductivity classification technique for nonmagnetic metal immune to tilt variations using eddy current testing, IEEE Access 9 (2021) 135334, https://doi.org/10.1109/ACCESS.2021.3116247.
[14] B. Cao, J. Sun, M. Fan, et al., Novel conductivity measurement of thin metallic materials using crossover frequency feature from triple-frequency eddy current signals, IEEE Trans. Instrum. Meas. 73 (2024) 6005611, https://doi.org/10.1109/TIM.2024.3383059.
[15] R. Huang, Z. Xia, M. Lu, Z. Zhang, et al., Model-based cylinder radius and permeability estimation using eddy current testing, Measurement 220 (2023) 113285, https://doi.org/10.1016/j.measurement.2023.113285.
[16] Z. Deng, Y. Wang, Q. Shi, et al., 2-D analytical model of sinusoidal eddy current field based on permeability distortion, IEEE Sens. J. 24 (9) (2024) 14392, https://doi.org/10.1109/JSEN.2024.3376804.
[17] G. Hu, R. Huang, M. Lu, L. Zhou, W. Yin, Measurement of radius of a metallic ball using eddy current testing based on peak frequency difference feature, Measurement 184 (2021) 109876.

[18] P. Huang, J. Long, J. Jia, K. Liu, et al., Measurement of conductivity and diameter of metallic rods using eddy current testing, Measurement 221 (2023) 113496, https://doi.org/10.1016/j.measurement.2023.113496.
[19] S. Babic, E. Guven, K.H. Song, Y. Luo, Optimized calculation of radial and axial magnetic forces between two non-coaxial coils of rectangular cross-section with parallel axes, Computation 12, 9 (2024) 180.
[20] G. Zhao, Y. Huang, W. Zhang, C. Wang, J. Chen, Advances in high-precision displacement and thickness measurement based on eddy current sensors: A review, Measurement 243 (2025) 116410, https://doi.org/10.1016/j.measurement.2024.116410.
[21] N. Praphaphankul, A. Akutsu, E. Sasaki, Numerical study for development of subsurface crack detection using pulsed eddy current and swept frequency eddy current, Struct. Infrastruct. Eng. 1 (2023), https://doi.org/10.1080/15732479.2023.2218351.
[22] G. Tytko, L. Dziczkowski, M. Magnuski, Z. Zhang, Y. Luo, Eddy current testing of conductive discs using the pot-core sensor, Sens. Actuators, A 349 (2023) 114060, https://doi.org/10.1016/j.sna.2022.114060.
[23] S. Zhang, Investigation of flux transfer along ferrite core of probe coil for eddy current nondestructive evaluation, Measure. Sci. Rev. 23 (1) (2023) 11–18.
[24] G. Tytko, Eddy current testing of conductive coatings using a pot-core sensor, Sensors 23 (2023) 1042, https://doi.org/10.3390/s23021042.
[25] G. Tytko, Locating defects in conductive materials using the eddy current model of the filamentary coil, *J. Nondestruct. Eval.* 40 (3) (2021) 66.
[26] Y. Xie, P. Huang, Y. Ding, J. Li, H. Pu, L. Xu, A novel conductivity measurement method for non-magnetic materials based on sweep-frequency eddy current method, *IEEE Trans. Instrum. Meas.* 71 (2022) 1–12.
[27] S. She, Z. Xia, X. Zheng, W. Yin, J. Shen, Simultaneous measurements of metal plate thickness and defect depth using low frequency sweeping eddy current testing, *Measurement* 233 (2024) 114687.
[28] Y. Li, Q. Xiao, L. Peng, S. Huang, C. Ye, A precise oxide film thickness measurement method based on swept frequency and transmission cable impedance correction, *Sensors* 25 (2) (2025) 579.
[29] Sangyul Ha, Saif Haider Kayani, Kyungjun Lee, Suwon Park, Hyunjoo Choi, Jae Bok Seol, Jung Gi Kim, Hyokyung Sung, Microscopic-plastic deformation behavior of grain boundary precipitates in an Al–Zn–Mg alloy, J. Mater. Res. Technol. 30 (2024) 3420–3429, https://doi.org/10.1016/j.jmrt.2024.04.044.
[30] Maria Inês Silva, Evgenii Malitckii, Telmo G. Santos, Pedro Vilaça, Review of conventional and advanced non-destructive testing techniques for detection and characterization of small-scale defects, Progr. Mater. Sci. 138 (2023) 101155, https://doi.org/10.1016/j.pmatsci.2023.101155.
[31] P.N. Quested, R.F. Brooks, L. Chapman, R. Morrell, Y. Youssef, K.C. Mills, Measurement and estimation of thermophysical properties of nickel based superalloys, Mater. Sci. Technol. 25 (2) (2009) 154–162, https://doi.org/10.1179/174328408X361454.
[32] S. Hillmann, M.H. Schulze, H. Heuer, High-Frequency Eddy Current Techniques, in: N. Ida, N. Meyendorf (Eds.), Handbook of Advanced Non-Destructive Evaluation, Springer, Cham, 2018, https://doi.org/10.1007/978-3-319-30050-4_49-1.
[33] N.G. Bychkov, V.P. Lukash, Y.A. Nozhnitsky, A.V. Perchin, A.D. Rekin, Investigations of thermomechanical fatigue for optimization of design and production process solutions for gas-turbine engine parts, Int. J. Fatigue 30 (2) (2008) 305–312, https://doi.org/10.1016/j.ijfatigue.2007.01.046.
[34] Mateusz Kopec, Ved Prakash Dubey, Marzena Pawlik, Paul Wood, Zbigniew L. Kowalewski, Experimental identification of yield surface for additively manufactured stainless steel 316L under tension–compression-torsion conditions considering its printing orientation, Manuf. Lett. 41 (2024) 28–32, https://doi.org/10.1016/j.mfglet.2024.07.003.